Electrical Power and Energy Systems 143 (2022) 108461

Contents lists available at ScienceDirect

International Journal of Electrical Power and Energy Systems

journal homepage: www.elsevier.com/locate/ijepes

A communication-free droop control scheme for distributed linear switched reluctance wave power generation system with adaptive voltage compensation

X.S. Jiang [a], Yue Hong [a], Kaiwen Chen [b], Norbert Cheung [a,b], Ka Wai Eric Cheng [b], J.F. Pan [a,*]

[a] Guangdong Key Laboratory of Electromagnetic Control and Intelligent Robots, College of Mechatronics and Control Engineering, Shenzhen University, Shenzhen 518060, China

[b] Power Electronics Research Centre, Department of Electrical Engineering, The Hong Kong Polytechnic University, HKSAR 999077, China

ARTICLE INFO

Keywords:
LSRG
Communication free droop control
Adaptive voltage compensation

ABSTRACT

In wave energy generation systems, scaled and improved energy extraction can be realized by utilizing distributed linear switch reluctant generators (LSRGs). However, this type of power generation system often employs supercapacitors (SCs) as the energy storage media, and the system often suffers from output voltage variation and current fluctuation from the LSRGs. Meanwhile, the fixed droop factor also causes bus voltage deviation and aggravates energy imbalance of the energy storage system. In this paper, a communication-free droop control scheme with adaptive voltage compensation is proposed for the distributed linear switched reluctance wave power generation system. First, system stability is improved by applying a high droop factor. When the bus voltage fluctuation exceeeds the compensator threshold, this voltage information of the energy storage unit is introduced into the control loop. In addition, an adaptive voltage compensation algorithm is proposed for the system, and the control algorithm is able to reduce the bus voltage deviation and the energy imbalance of the storage unit, caused by the droop factor. The proposed control strategy can further improve the response and reliability of the energy storage units, and the bus voltage fluctuation can be regulated within ±3%.

1. Introduction

As a clean renewable energy source, ocean wave energy is characterized by a wide spread distribution, high energy density, and abundant global reserves [1]. Nowadays, wave energy extraction technologies mainly focus on indirect wave energy conversion methods. Some commercialized wave energy converters (WECs) employ mechanical translations, such as air and hydraulic turbines, to generate electricity by converting the low-speed wave motion into high-speed rotation movement. The commercial WECs include Pelamis of Ocean Power Delivery, wave dragon from Wave Dragon APS, and BV-AWS's Archimedes Wave Swing, etc. However, the method of indirect wave energy extraction often leads to a complex power generation system with low overall conversion efficiency [2,3], and the indirect ways of power generation by WECs are not cost-effective. Consequently, the-state-of-art WECs are not yet widely employed in large-scale wave power generation applications.

Recently, the direct-drive WECs approaches are investigated. By the utilization of linear generators, system complexity caused by intermediate mechanical converters can be eliminated. As a result, the direct-drive approach contributes to a simpler power output system at higher power efficiency [4]. Current research focuses on linear permanent magnet synchronous generators (LSPMGs). Although LSPMGs have relatively large force-to-volume ratios and high conversion rates, the invovlmen of permanent magnets (PMs) requires complex arrangements [5]. In addition, the assemblies of PMs often leads to a high overall manufacturing and assembly cost [6]. In addition, humidity and temperature variations from the marine environment may cause system degradation or even cause failure in the LSPMG based power generation system [7]. As an ideal alternative, a linear switched reluctance generator (LSRG) is suitable for the operation in hostile environments [4]. The LSRG only contains laminated steel sheets and copper wires, and the total mass manufacturing cost is very low. Due to the absence of PMs or complex windings, the LSRG is very suitable to construct distributed wave power generation system in a large scale [8,9]. However, the LSRG produces pulsating direct current which results in an unstable power

* Corresponding author.
E-mail address: pan_jian_fei@163.com (J.F. Pan).

https://doi.org/10.1016/j.ijepes.2022.108461
Received 28 December 2021; Received in revised form 1 June 2022; Accepted 29 June 2022
Available online 7 July 2022

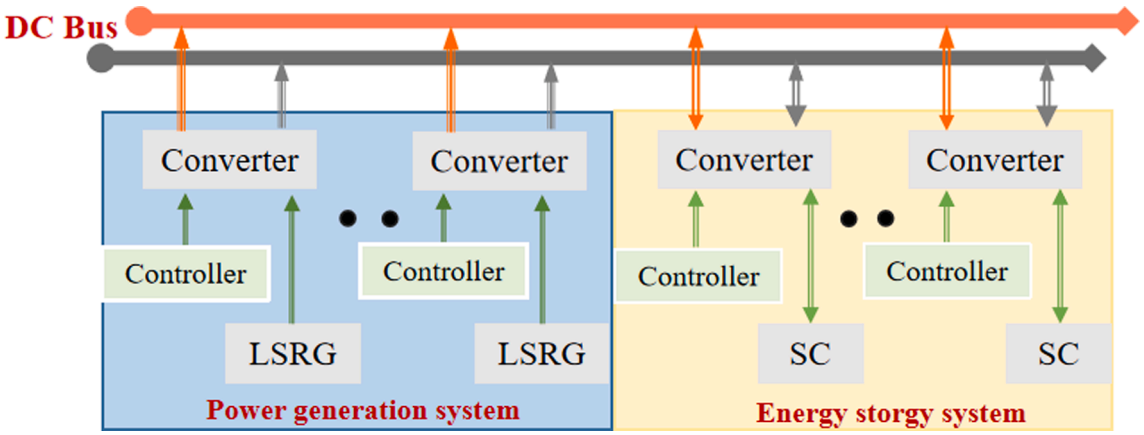

Fig. 1. Schematic diagram of distributed generation system and energy storage system.

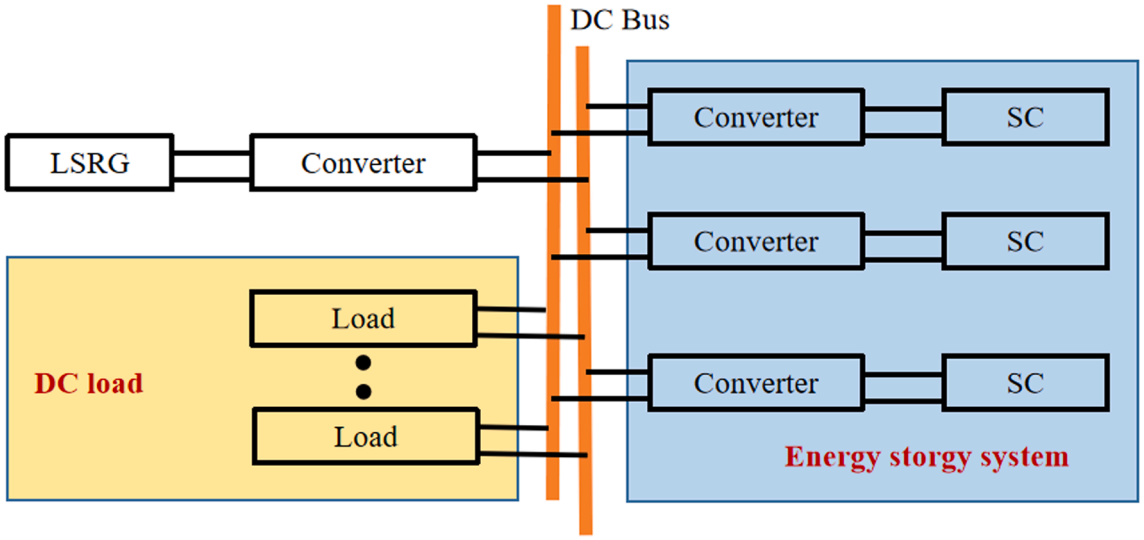

Fig. 2. Structure of the distributed LSRGs system.

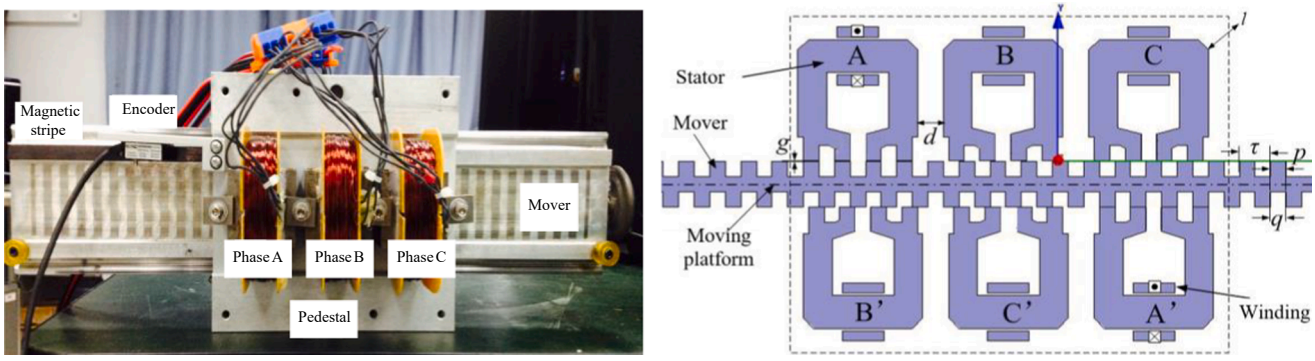

(a) (b)

Fig. 3. (a) Physical picture of LSRG; (b) LSRG structural cross section.

supply and the LSRG based power generation system is more difficult to control.

Supercapacitors (SCs) are very suitable for the storage of instantaneous power, due to their high power density and durability [10]. This paper investigates direct-drive generators based WEC system which includes distributed LSRGs and SCs for power generation and energy storage. As shown in Fig. 1, each distributed LSRG unit is connected to the direct current (DC) bus. Compared to the centralized structure, the main features of the distributed structure can be characterized as: (a) each distributed unit has an independent controller and the entire system is fault-tolerant [11]; (b) since there is no centralized controller, the spatial arrangement of each distributed unit is flexible; (c) the

Table 1
Parameters of LSRG.

Parameters	Values
Number of turns winding coil	220
Phase winding resistance	2 Ω
Polar distance	12 mm
Slot width	6 mm
Air gap width	0.3 mm
Kinetic length	350 mm
Stator distance	10 mm

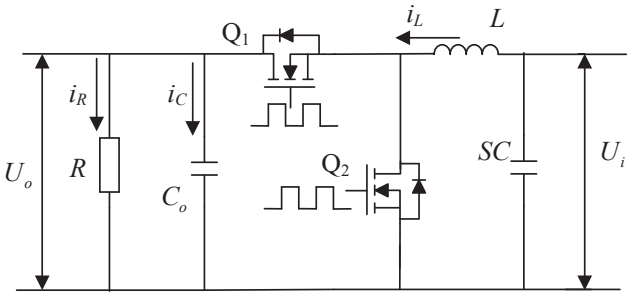

Fig. 4. Circuit of the energy storage unit.

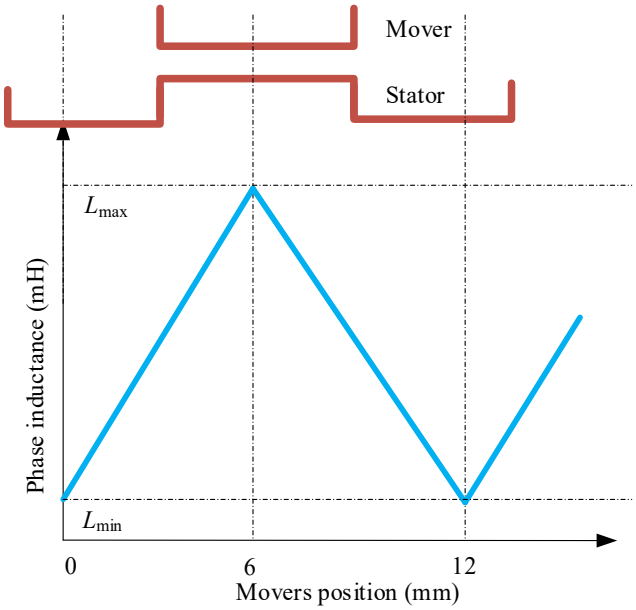

Fig. 5. Linear model diagram of phase inductance.

distributed units can be modularized, so the distributed system can be scalable [11]. However, the absence of a centralized controller may lead to the unbalanced flow of energy among the energy storage units [12].

Conventional droop control can improve current equalization in energy storage units in distributed DC microgrids [13]. However, conventional droop control has its limitations, such as inaccurate current distribution and deviation of the bus voltage, caused by the converter line impedance. The deviations in bus voltage may cause damage to the load and the instability of the overall system as well. Some research work has been carried out to minimize bus voltage deviations. A piecewise linear droop mechanism is applied to modify the droop factor in different voltage bands, however, the limited droop factor values cannot satisfy variable load conditions [6]. The idea is further developed in [14], and the droop factor continuously varies in response to the change in the power level. The steady-state value of the bus voltage is maintained within ±3% of the reference value, when the load variation is suddenly doubled. However, the improved voltage regulation can aggravate the imbalance in the energy storage unit [15]. To solve the energy imbalance problem from the energy storage units, there are different approaches to realize the current distribution of the load, according to the power of the energy storage unit, such as the adaptive droop control methods [16,17]. Current sharing loops are applied in the adaptive droop control for online updating of the droop resistance for each unit in the energy storage system. Classical proportional-integral (PI) controllers are employed to the droop parameters. This approach requires the share of the unit currents in the different controllers through low-bandwidth communication networks. However, the control algorithm has a complex structure and poor stability [18]. To simplify control complexity, a soft-switching balance technique is proposed in [19], and the balance strategy employs an isolated converter to transfer the energy from the high state of charge (SoC) units to the low SoC units. With the increase of energy storage units, the number of converters increases and this leads to a complex system structure. Therefore, the above algorithms are not able to satisfy the expected bus voltage in case of high load conditions [20].

Researchers currently focus on control schemes that can simultaneously eliminate bus voltage drops and improve the energy imbalance of storage units [21]. By modifying the droop factor, the bus voltage deviation and the energy imbalance of the storage unit can be reduced. The SoC of the energy storage unit and the load power are introduced into the droop controller [22,23], and this method relies only on the modifications of the droop factor to achieve the above two control objectives. The droop factor is determined by two parameters, which leads to poor dynamic performance and stability of the system [24]. Scholars have also combined optimization algorithms with the hierarchical control algorithm [25,26]. The hierarchical control algorithm is a classification of the entire control method into three levels, and two controllers are added to eliminate bus voltage drop and energy flow of each unit. The hierarchical controllers are typically implemented in a centralized fashion [27], where a central entity communicates with the converters through a high band communication network. Loss of any link in such topologies can lead to the failure of the corresponding unit and influence the performance other units, and potentially result in system-level instability and cascaded failures [28].

The distributed control strategy without communication has recently aroused researchers' interests [29]. A communication-free adaptive droop control method can automatically adjust the droop factor according to load situations [30]. This method can increase the robustness of the control system, and enable multiple energy storage units to reach an energy balance state. However, the algorithm requires solving complex droop control equations in real-time. Recently, many swarm intelligence-based optimization methods have been applied to find the optimal values of the droop factor, such as particle swarm optimization (PSO) and the genetic algorithm [31]. Nevertheless, the heavy computational burden of the optimization algorithms prevents its online implementation. The above-mentioned communication-free control algorithm can achieve energy equalization among multiple energy storage units by modifying the droop factor. However, when the system is connected to a heavy load, the above algorithm does not take into account the voltage drop caused by the droop factor [32]. When the voltage drop exceeds 10% of the reference value, the load can even be damaged.

This paper proposes a novel droop control strategy to integrate an adaptive state feedback into the conventional droop control for the distributed LSRGs power generation with SCs energy storage. The ultimate goal of this control scheme is to smooth the output voltage of the LSRG and equalize the SoC of each energy storage unit. Specifically, the SoC information of the energy storage unit is applied as a factor to set the reference value of the bus voltage. The contributions of this paper can be summarized as follows. First, a distributed energy storage and generation system with LSRGs and SCs is adopted in this paper. The system

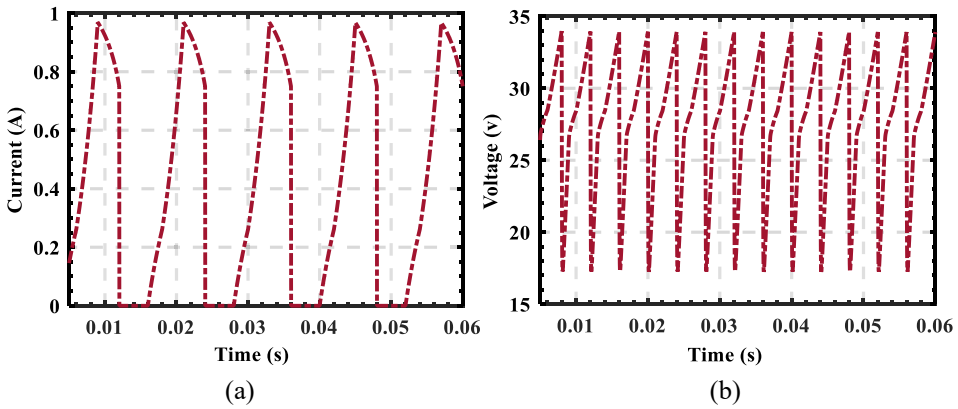

Fig. 6. (a) Output voltage of LSRG; (b) Phase current of LSRG.

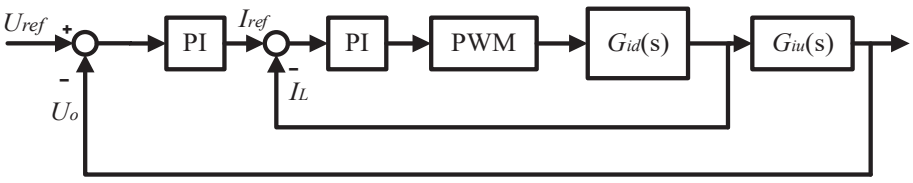

Fig. 7. The constant voltage control diagram.

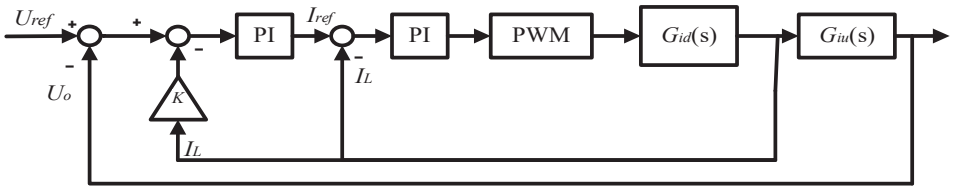

Fig. 8. Droop control diagram.

offers high stability and power generation efficiency. Second, a novel communication-free droop control algorithm is proposed, which can solve the problems of bus voltage drops and the energy imbalance of energy storage units.

2. Modeling of the LSRGs system

The structure of the proposed distributed LSRGs system can be found in Fig. 2. The LSRG and storage units are connected to the direct current (DC) bus in parallel. This structure has the characteristics of high efficiency, high reliability, and flexible control [7].

2.1. The structure of LSRG

The picture and the schematic structure of the LSRGs can be found in Fig. 3 (a) and (b). The LSRG employs an asymmetric structure, where the double-sided stators are not symmetric according to the axis. This electromagnetic structure has the advantages of a higher force-to-volume ratio and efficiency [4]. The moving platform is supported by a pair of linear guides. Each phase of the LSRGs has the same dimensions and ratings and the phases are defined as AA′, BB′, and CC′, respectively. The main specifications of LSRG unit are summarized in Table 1.

2.2. Mathematical model of LSRG

LSRG can be considered as a typical energy conversion system. From the mechanical side, the motion equation can be represented as,

$$F = M\frac{d^2x}{dt^2} + D\frac{dx}{dt} + f \tag{1}$$

where F is the mechanical force input; M is the mass of the mover track; D is the friction coefficient. f stands for the electromagnetic force and x is the position of the mover. The electrical equations of LSRG can be described as (2),

$$u_k = R_k i_k + \frac{d\lambda_k}{dt} \quad (k = AA',\ BB',\ CC') \tag{2}$$

where $\lambda_k = i_k L_k$ is the total magnetic chain of the k-th phase winding of the LSRG unit. u_k, R_k, L_k, and i_k are the voltage drop, phase resistance, phase inductance, and phase current of the k-th phase winding of the motor, respectively. According to (2), it can be further obtained as,

$$u_k = R_k i_k + [\frac{\partial L_k}{\partial i_k} i_k + L_k]\frac{di_k}{dt} + v_x \cdot \frac{\partial L_k}{\partial x} \cdot i_k \quad (k = AA',\ BB',\ CC') \tag{3}$$

$$v_x = \frac{dx}{dt} \tag{4}$$

The electromagnetic force can be calculated by the following equation,

$$f(i_k, x) = \frac{\partial W_c(i_k, x)}{\partial x} = \frac{1}{2}\sum_{k=\mathrm{AA'}}^{\mathrm{CC'}} (i_k^2 \frac{dL_k}{dx}) \quad (k = AA',\ BB',\ CC') \tag{5}$$

The mathematical model of LSRG can be described by the following equations,

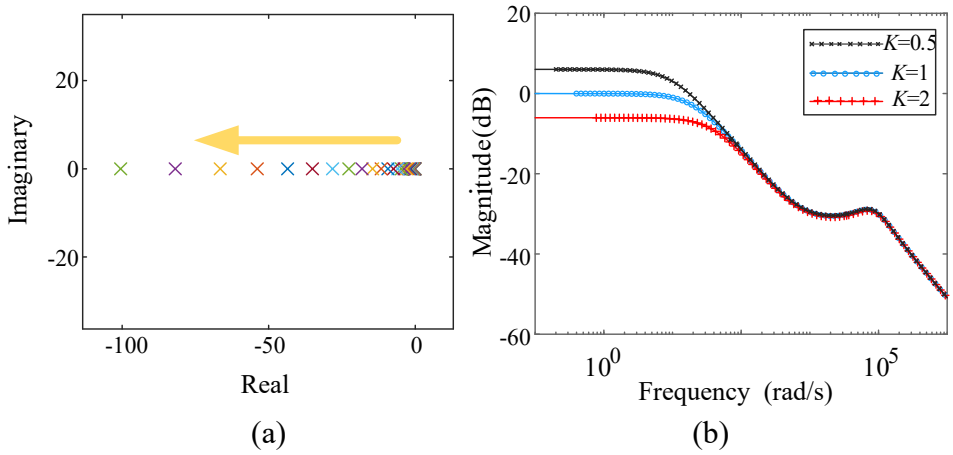

Fig. 9. (a) Partial root trajectory of the system; (b) Amplitude and frequency curves of the system.

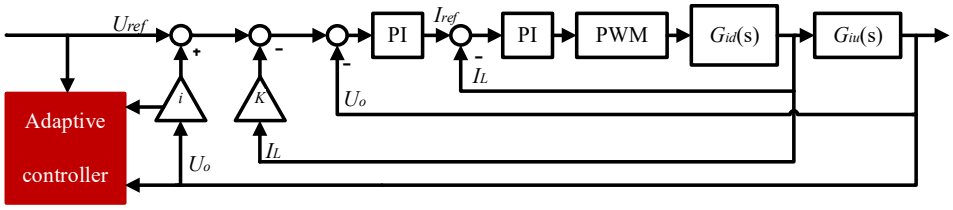

Fig. 10. Control block diagram of the energy storage system.

$$\begin{cases} u_k = R_k i_k + [\dfrac{\partial L_k}{\partial i_k} i_k + L_k]\dfrac{di_k}{dt} + v_x \cdot \dfrac{\partial L_k}{\partial x} \cdot i_k \\ f(i_k, x) = \dfrac{\partial W_c(i_k, x)}{\partial x} = \dfrac{1}{2}\sum_{k=\mathrm{AA}'}^{\mathrm{CC}'} (i_k^2 \dfrac{dL_k}{dx}) \quad (k = AA',\ BB',\ CC') \\ F = M\dfrac{d^2x}{dt^2} + D\dfrac{dx}{dt} + f \\ v_x = \dfrac{dx}{dt} \end{cases} \tag{6}$$

When $\partial L_k/\partial x < 0$, LSRG enters the power generation state. If $-u_k - v_x \cdot \partial L_k/\partial x \cdot I > 0$ is satisfied, the k-th phase current of LSRG will exceed the excitation current. In order to obtain a more accurate value of the generator phase current, the current variation law can be deducted from (3) and (5) and the bus voltage of the LSRG is assumed to be constant. When the LSRG is excited, the changing rate of the phase current relative to the mover position can be described as follows,

$$\frac{di_k}{dx} = \frac{U_b - 2U_T}{v_x \cdot L(i_k, x)} - \frac{\frac{\partial \lambda(i_k, x)}{\partial x} \cdot v_x + R}{v_x \cdot L(i_k, x)} \cdot i_k(x) \quad (k = AA',\ BB',\ CC') \tag{7}$$

The output pulsating current of the LSRG is shown in (7) and it is clear that the frequency of the pulsating current is related to the operating speed of the motor.

2.3. Mathematical model of the energy storage unit

As shown in Fig. 4, the energy storage unit consists of an SC with a bidirectional converter. To obtain a good dynamic performance of the control system, the small signal modeling method of the converter is employed. In Fig. 4, u_L and i_L are the voltage and current of the inductor respectively; u_c and i_c are the voltage and current on the capacitor respectively; U_i and U_o are the input and output voltages of the converter respectively; R and i_R are the resistance and current of the resistor that is connected to the converter, respectively.

The operation of the converter can be summarized as follows. When Q_2 is off and the duty cycle of Q_1 control signal is d, the current flows from U_o to U_i, SC is charging. When Q_1 is off and the duty cycle of Q_2 control signal is d, the current flows from U_o to U_i. When SC is discharging, the volt-ampere relationship between the two energy storage units in the circuit can be analyzed as follows.

$$\begin{cases} u_L = U_i = L di_L/dt \\ i_C = -u_L/R = C du_C/dt \end{cases} \tag{8}$$

When Q_2 is turned off, the volt-ampere relationship between the two energy storage units in the circuit is shown in the following equation,

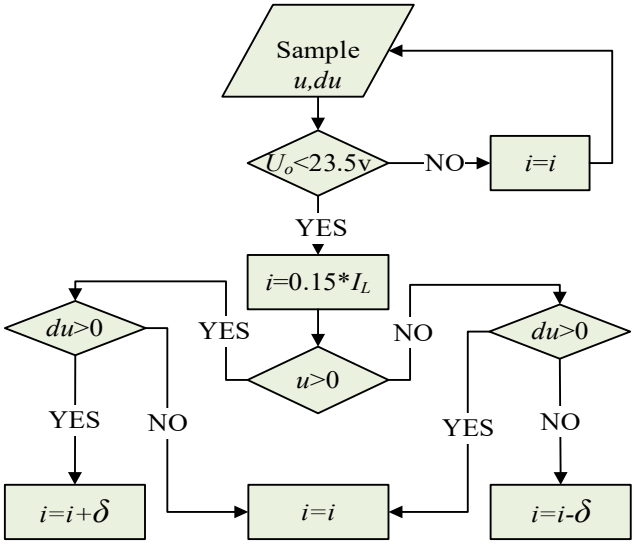

Fig. 11. Flowchart of the control algorithm.

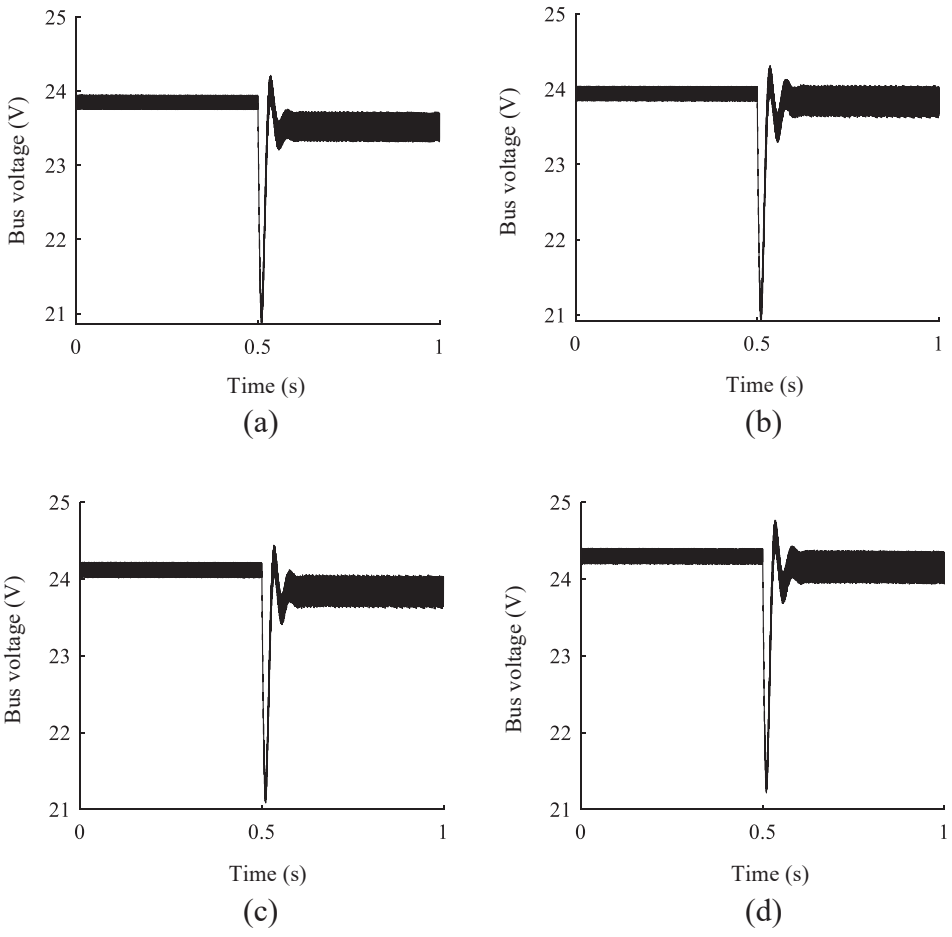

Fig. 12. (a) Threshold voltage is 23.2 V, (b) Threshold voltage is 23.4 V, (c) Threshold voltage is 23.6 V, (d) Threshold voltage is 23.8 V.

$$\begin{cases} u_L = U_i - U_O = L di_L/dt \\ i_C = i_L - u_L/u_L R = C du_C/dt \end{cases} \tag{9}$$

If we assume that the current value on the inductor and the voltage value across the capacitor remain constant during one switching cycle of the pulse width modulation (PWM) scheme, the above equations can be derived in S domain,

$$\begin{cases} U_i - (1-d)U_O = Lsi_L \\ (1-d)i_L - u_C/R = Csu_c \end{cases} \tag{10}$$

The above equations demonstrates the volt-ampere relationship on the inductor and capacitor at a single cycle. In order to obtain the state quantities of the inductors and capacitors in the converter, the small-signal model of the converter should be derived. The variables in (10) are divided into a constant signal and a fluctuating signal. The expression is shown as,

$$\begin{cases} i_L = I_L + i_L^{'} \\ u_C = U_C + u_C^{'} \\ d = D + d^{'} \end{cases} \tag{11}$$

where I_L and i_L' are the direct current (DC) and alternating current (AC) components of the inductor current, respectively; U_c and u_c' are the DC and AC components of the capacitance voltage, respectively; D and d' are the DC component and AC component of the duty cycle signal, respectively. Substituting (11) into (10), we can get (12),

$$\begin{cases} U_i - (1-D-d^{'})U_O = Ls(i_L^{'} + I_L) \\ (1-D-d^{'})(i_L^{'} + I_L) - (U_C + u_C^{'})/R = Cs(U_C + u_C^{'}) \end{cases} \tag{12}$$

When the system reaches a steady state, the relationship between D, U_c, and I_L can be deducted as shown in (13) below,

$$\begin{cases} U_i - (1-D)V_O = LsI_L \\ (1-D)I_L - U_C/R = CsU_C \end{cases} \tag{13}$$

Substituting (13) into (12), the small signal model of the system can be depicted as (14) below,

$$\begin{cases} -(1-D)u_C^{'} + d^{'}U_C = Lsi_L^{'} \\ (1-D)i_L^{'} - d^{'}I_L = (Cs + 1/R)u_C^{'} \end{cases} \tag{14}$$

From the above small signal model analysis, the transfer functions of the system can be deduced. The result is shown in (15) below,

$$\begin{cases} G_{di} = \dfrac{U_O Cs + 2U_O/R}{LCs^2 + (L/R)s + d''^2} \\ G_{iv} = \dfrac{d''^2 R - Ls}{d''RCs + 2d''} \end{cases} \tag{15}$$

When the converter is operated in Buck mode, the transfer function of the system can be obtained from the above approach as shown in (16) below.

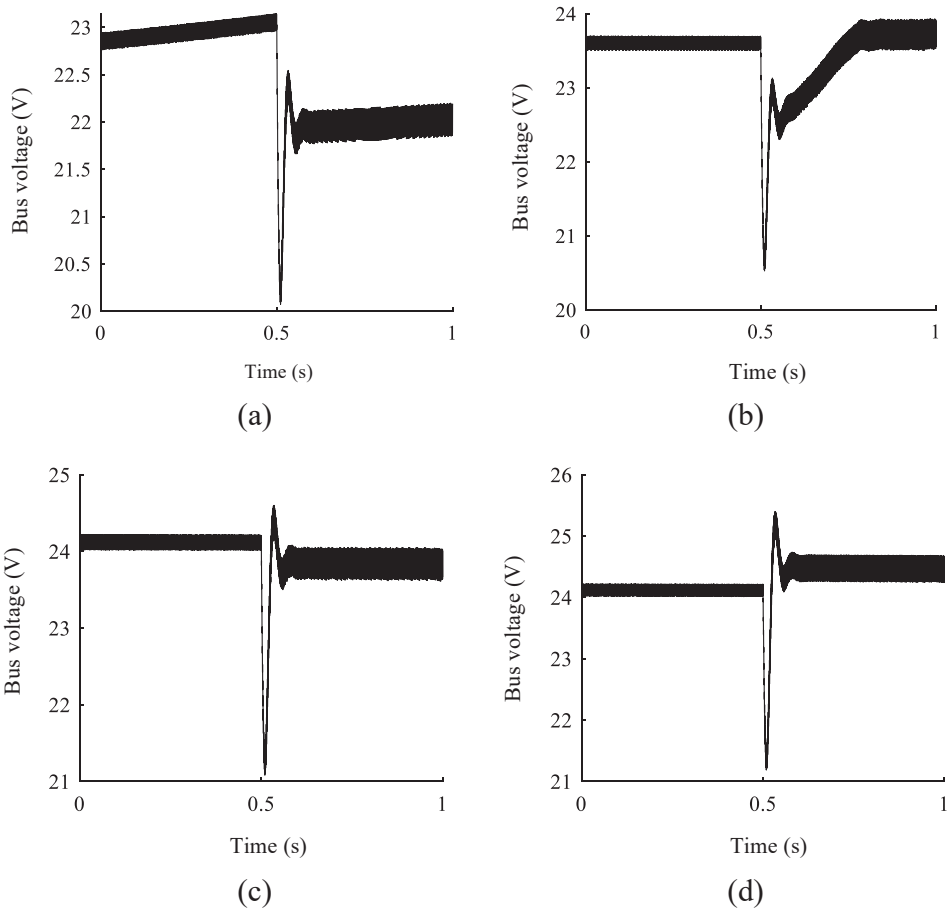

Fig. 13. (a) $\delta = 0.0001$, (b) $\delta = 0.0005$, (c) $\delta = 0.001$, (a) $\delta = 0.002$.

$$\begin{cases} G_{di} = \dfrac{U_i RCs + U_i}{LCRs^2 + Ls + R} \\ G_{iv} = \dfrac{R}{RCs + 1} \end{cases} \tag{16}$$

3. Control strategy of the system

In this paper, a bidirectional converter is employed as the voltage converter for the energy storage system. As shown in Fig. 4, when Q_1 of the converter turns on and Q_2 turns off, it is a Buck converter circuit and the bus voltage flows into the energy storage unit. When Q_2 of the converter is turned on and Q_1 is turned off, the circuit topology is a Boost converter circuit and the energy storage units provide energy to the DC bus. The operating mode of the bidirectional converter is determined by the bus voltage value. When the bus voltage is greater than the reference voltage value, the bidirectional converter operates in Buck mode; The bidirectional converter operates in Boost mode if the bus voltage is less than the reference. Therefore, the controllers of Buck and Boost circuits are required to be designed separately.

3.1. Constant voltage controller design

In this paper, a single LSRG generator is applied and the rated speed v of the motor is 1 m/s. The current pulsation frequency f generated by the LSRG is shown in (17).

$$f = 3v/\tau \tag{17}$$

where τ is the motor's pole pitch of 12 mm. When the LSRG is generating power at an expected speed, the current pulsation frequency is 250 Hz, and the resulting voltage fluctuation frequency is also 250 Hz.

Fig. 6 (a) and (b) show the output current and output voltage for a single phase of the LSRG, respectively. The phase inductance L is linearly related to the mover position as shown in Fig. 5. It can be seen that the output current and voltage of the LSRG fluctuate more than 25% of the stable value.

As shown in Fig. 7, a dual-loop voltage controller is applied to the control system. The current of the SC is adopted as a reference input to control the inner loop, and the input reference for the control outer loop is the bus voltage. Combined with the small-signal model of the system shown in (15), the parameter design principle of the inner-loop is that the cutoff frequency is less than one-fifth of the switching frequency of the system. Therefore, the cut-off frequency and the phase angle margin of the current inner loop are chosen to be 2 kHz and 60°, respectively. The cut-off frequency of the system voltage loop is also not higher than one-fifth of the current loop cut-off frequency. In order to suppress the voltage fluctuation generated by the switched reluctance generator, the voltage loop cutoff frequency is set to 200 Hz and the phase angle margin is 60°, respectively. In Fig. 7, U_{ref} is the reference voltage of the DC bus; U_{dc} is the voltage setting value of DC bus; G_{iu} is the transfer function between inductive current and bus voltage; G_{id} is the transfer function between duty cycle of control signal and inductive current; U_o and I_L are the voltage of SCs and the current of filter inductance, respectively.

The principle of the selection of the controller parameters in Boost mode is the same as that in Buck mode. However, when the SC voltage is low, an excessive output current is required to match the power to be compensated with the bus voltage. When the inductor current in the converter is enabled, the high output current will cause a huge voltage spike in the inductor. This will result in poor system stability and can aggravate the energy imbalance between the energy storage units. The

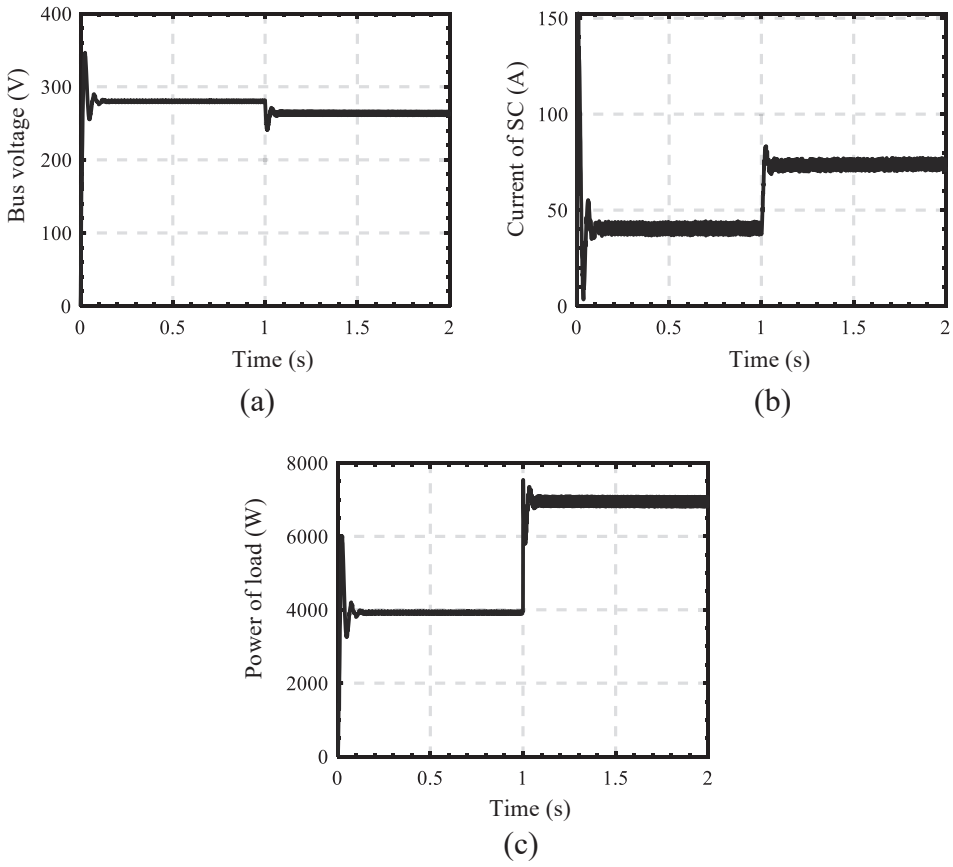

Fig. 14. Result of conventional droop control, (a) Bus voltage; (b) Current of SC; (c) Power of load.

voltage controller output of this system is limited to 6 A and the voltages of SCs should be more than 5 V.

3.2. Droop factor design

As shown in Fig. 8, a constant droop factor K is employed in the droop control algorithm and the droop factor determines stability and the dynamic performance.

When the converter is operating in Boost mode, Fig. 9 (a) shows the root trajectory of the system as the droop factor increases from 0 to 5. It can be seen that the dominant pole of the system is always located in the left half-plane of the S domain. As the value of K increases, the farther the dominant pole is from the imaginary axis, the more stable the system is. The amplitude and frequency curve of the system is shown in Fig. 9 (b) below. As the value of K increases, the amplitude curve in the low frequency region of the system falls, thus causing the steady-state performance of the system to deteriorate.

The poor stability of the control system can be caused by the droop control factor with a small value. However, a high value of the droop factor can lead to a large drop in bus voltage and a poor dynamic performance of the system. As shown in Fig. 9 (a), the larger value of K, the closed-loop pole of the system deviates from the imaginary axis, the better stability and rapidity of the control system can be guaranteed. In addition, the larger value of K, the smaller value of low frequency band, the larger steady-state error of the closed-loop system and the lower the steady-state accuracy of the system can be obtained. When $K = 1$, the amplitude of low-frequency curve is 0. When $K = 0.5$, the low-frequency amplitude of the system is greater than 5 dB, and the control system has good steady-state accuracy and stability. In order to suppress the pulsation generated by the LSRG generation, the droop factor of the bidirectional converter operating in Boost mode is set to 0.5. Similarly, it is deduced that the droop factor of the bidirectional converter operating in Buck mode is set to 0.5.

The relationship between the output voltage and current can be characterized as follows,

$$V_o = V_{\text{ref}} - KI_o \tag{18}$$

3.3. Adaptive voltage compensation controller

In order to solve the problem of bus voltage drops and energy imbalance in the conventional droop control, an adaptive voltage compensation control is introduced into the droop control loop. In the Buck and Boost modes, the control block diagram of the system is shown in Fig. 10. The control system is introduced with the adaptive voltage compensation scheme based on a double closed-loop PI controller and the adaptive control algorithm employs the bus voltage as the threshold of the voltage compensation algorithm. The value of the adaptive voltage compensation factor is then applied at the beginning of each control cycle, according to the direction and the trend of the voltage deviation. In this case, the value of the voltage compensation factor for each energy storage unit is reset according to the output current value of the SC, whenever the fluctuation value of the bus voltage is less than the algorithm turn-on threshold of the system. The voltage compensation factor is configured to avoid the fluctuation when the bus voltage stabilizes, and the compensation factor can further reduce bus voltage fluctuation. The algorithm proposed in this paper can fully take into account the bus voltage drop value. In addition, the voltage of the energy storage unit is introduced into the algorithm. Therefore, higher voltage of the SCs will enable more current on charging and discharging of the SCs.

Since the open-loop transfer function of Boost mode contains a zero point in the right half-plane of S, the stability and dynamic performance is worse compared to that from the Buck mode. Therefore, this paper

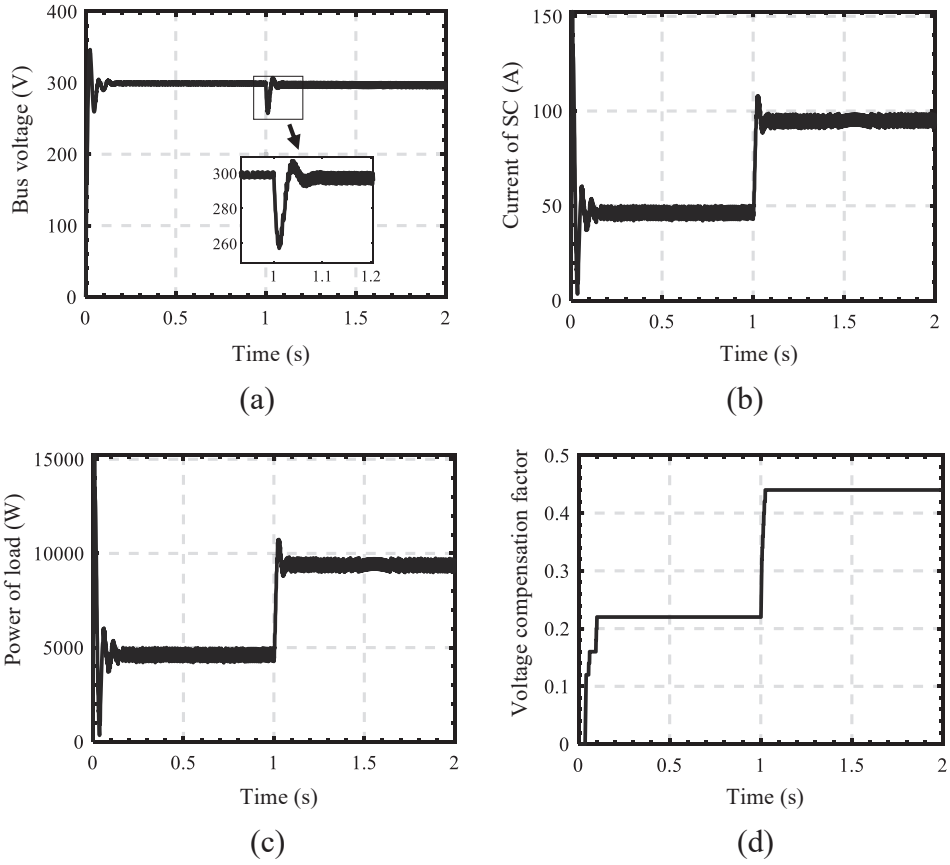

Fig. 15. Result of adaptive voltage compensation droop control, (a) Bus voltage; (b) Current of SC; (c) Power of load; (d) Voltage compensation factor.

focuses on the droop control with adaptive voltage compensation in Boost mode. When the bus voltage value drops under the threshold of the set value, the factor of adaptive voltage compensation is calculated by the following equation (19) and the flow chart of the control system is shown in Fig. 11.

$$\begin{cases} i = i + \delta\{ \begin{matrix} du > 0; \\ u > 0; \end{matrix} \\ i = i - \delta\{ \begin{matrix} du < 0; \\ u < 0; \end{matrix} \\ i = i; (\text{else}) \end{cases} \tag{19}$$

The turn-on threshold voltage is U_o, and the offset of the voltage compensation factor is δ. u is expressed as the amount of deviation of the bus voltage, i.e, U_{ref} - U_o, and du stands for the derivative of u.

3.4. Parameter selection of the adaptive voltage compensator

The effect of the compensation controller is limited by two new impact factor algorithms to the turn-on threshold and the offset of the voltage compensation factor.

In order to verify the influence of threshold voltage on bus voltage, four comparative simulations of threshold voltage are constructed in this paper. The result from Fig. 12 demonstrates that, the large threshold voltage improves the steady-state accuracy of bus voltage. However, a high threshold voltage may cause false switching of the converter operating mode. Therefore, the threshold voltage of 23.6 V is selected in this paper.

The turn-on threshold voltage of U_o cannot be a very big value, otherwise it will cause the bus voltage to fluctuate around the threshold. With a smaller U_o, the compensator cannot be effectively utilized. In order to ensure that the proposed algorithm is suitable for all LSRG power generation systems, the selection of U_o is discussed as follows. The choice of U_o depends on the accuracy of the supply voltage required by the load. Since the fluctuation from the supply voltage of the common DC load should not exceed 5%, U_o should be greater than the voltage value after 5% of the bus voltage drop, i.e., U_o should be greater than 22.8 V. When the fluctuation value of the bus voltage is set below 1% of the reference voltage, the compensation controller does not function, so U_o should be less than 23.76 V, and the selection range of U_o is thus 22.8–23.76 V. When the steady-state accuracy of the bus voltage is required to be increased, the variation range of δ can be limited as U_o is fixed, in order to ensure the working state of the energy storage converter is not influced by the change from U_o.

When $u > 0$, the first-order derivative of the bus voltage is increasing; When du > 0, the second-order derivative of the bus voltage is increasing. δ is set as the change in voltage compensation factor per unit time. In order to verify the influence of δ on bus voltage, four comparative simulations of δ are set up in this paper. The result can be found in Fig. 13 and it can be concluded that a large δ value increases the overshoot of the system. Therefore, δ is selected as 0.001.

In order to ensure that the proposed algorithm is suitable for all LSRG power generation systems, the selection of δ is investigated. The choice of δ values requires to consider the response speed and stability of the system simultaneously. Since the rated voltage of the SC is 10 V, the maximum variation of the output of the compensation controller is 10 times of δ. The sampling frequency of the compensation controller is 1 kHz. When the compensation controller is introduced, the bus voltage fluctuation needs to be compensated to be within 5% of the reference voltage for 0.1 s. First, the maximum deviation of the bus voltage is calculated according to the rated output current of the energy storage unit, and then the compensation value of the bus voltage can calculated. The continuous increasing or decreasing range of the compensation

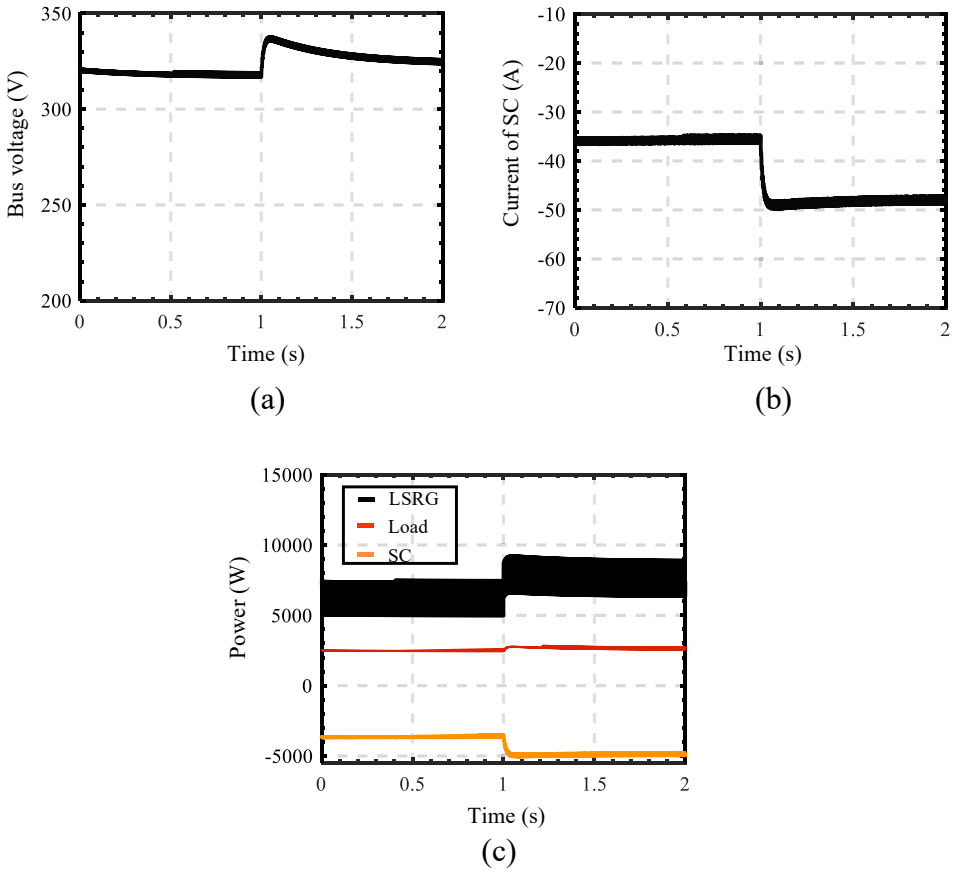

Fig. 16. Result of conventional droop control, (a) Bus voltage; (b) Current of SC; (c) Power of SC, load and LSRG.

coefficient value within 0.1 s should be bigger than the compensation value of the bus voltage, in order to determine the lower limit of δ. The bigger the value of δ is, the faster the dynamic response of the system will be. However, a bigger δ value will cause a large single output fluctuation of the compensation controller, thus affecting the stability of the system. Therefore, the maximum value of δ should be selected to improve the response speed of the system, and at the same time, the change value of the single compensation coefficient should be less than 1% of the bus voltage.

4. Analysis of simulation and experimental results

4.1. Simulation comparison and result analysis

The initial conditions of simulation are: the power of LSRG is 0 W, the initial voltage of SC is 100 V, and the load variates from 20 Ω to 10 Ω at 1 s. A comparison of conventional droop and the proposed control strategy with the adaptive voltage compensation results is shown in Figs. 14 and 15, respectively. As shown in Fig. 14, before 1 s, the rated power of load is 4500 W and the actual power is 3800 W. At this time, SC discharge current is 38 A, the bus voltage drops to 281 V, and the bus voltage deviation is greater than 5% of the reference value. After 1 s, the rated power of the load increases to 9000 W and the actual power is 6500 W. At this time, SC discharge current increases to 66 A, the bus voltage drop to 268 V, and the bus voltage deviation is higher than 16.7% of the reference value, which can not supply power to the load sufficiently.

As shown in Fig. 15, the rated power of load is 4500 W and the actual power is 4500 W. The discharge current of SC is 45 A and the voltage compensation factor is 0.22. The bus voltage is 298 V, and the bus voltage deviation does not exceed 1% of the reference voltage. After 1 s, the bus voltage decreases with the increase of the load power. The increase of the compensation factor compensates the bus voltage to 295 V, and thus the bus voltage deviation does not exceed 2% of the reference value.

Compared with the traditional droop control, the proposed algorithm compensates for the decrease of bus voltage and shortens the regulation time when the load power increases, and the steady-state accuracy of bus voltage is improved by 14.8%, which can provide stable power to the load.

When the output power of LSRG is higher than that of the load power, the excess energy is stored in the energy storage equipment. The initial conditions of simulation are: LSRG output power changes from 6000 W to 8000 W in 1 s, the SC initial voltage is 100 V, and the load is 40 Ω. A comparison of the conventional droop and proposed control strategy with the adaptive voltage compensation results is shown in Figs. 16 and 17, respectively.

As shown in Fig. 16, the rated power of load before 1 s is 2250 W and the actual power is 2400 W, the charging current of SC is 36 A, the bus voltage is 318 V, and the bus voltage deviation is 6% higher than the reference value. After 1 s, the generation power increases, the SC charging current increases to 48 A, the bus voltage is 325 V, and the bus voltage deviation is 8% higher than the reference value.

As shown in Fig. 17, the bus voltage before 1 s is 301 V, and the bus voltage deviation does not exceed 1% of the reference voltage. The SC charging current is 36 A and the compensation factor is 0.24. After 1 s, as the generation power increases, the charging current of SC increases, the compensation factor increases from 0.24 to 0.28, and the bus voltage reaches a stable state of 309 V within 0.3 s.

In the charging simulation of energy storage system, when the output power of generation system is 8000 W, the regulation time of the proposed algorithm is reduced and the steady-state accuracy of bus voltage is improved by 6.3%.

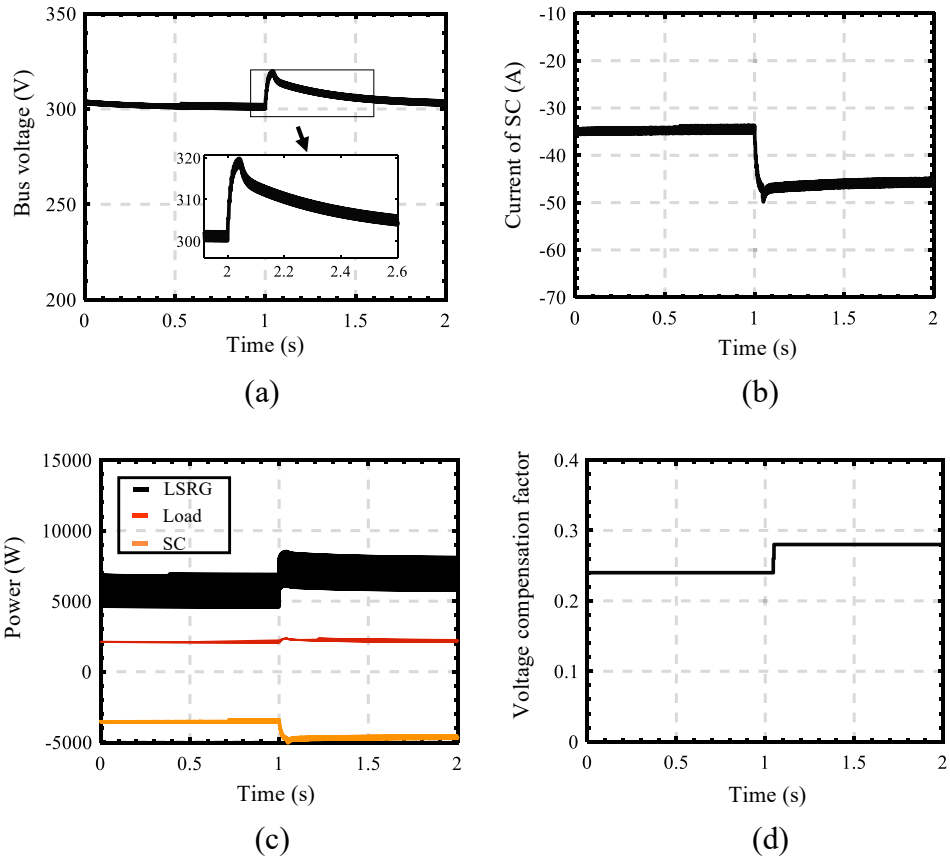

Fig. 17. Result of adaptive voltage compensation droop control, (a) Bus voltage; (b) Current of SC; (c) Power of SC, load, LSRG; (d) Voltage compensation factor.

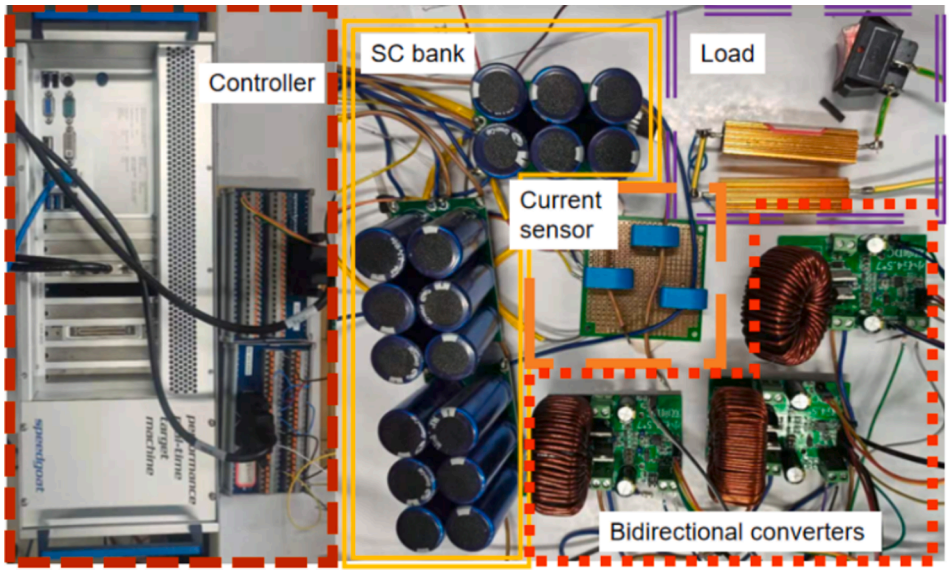

Fig. 18. Physical diagram of the energy storage system.

4.2. Experimental setup

This section investigates the performance comparison of the proposed droop control algorithm with adaptive voltage compensation to the conventional droop control algorithm in terms of anti-disturbance capability and energy equalization. As shown in Fig. 18, the hardware in loop controller (Speedgoat®) is adopted in this experiment, where the sampling rate is 10 kHz and the control frequency is 2 kHz, respectively. The SC bank is employed as the energy storage device, the bidirectional converter is responsible for energy transmission energy between the SC and DC bus. The main parameters of the bidirectional converter and SC are shown in Table 2.

4.3. Experimental results

The operation mode of the wave power generation and energy

Table 2
Wave power generation system parameters.

Parameters	Symbol	Value
Output power	P_o	0–50 W
Output voltage	V_o	24 V
ON-state resistance of MOSFET	r_{DS}	4.8mohm
ON-state resistance of diode	r_f	1mohm
Filter inductor	L	1mH
Filter capacitor	C	680uF
Nominal switching frequency	f_{sw}	20 kHz
SC(Super Capacitor)	C_{sc}	18F
ESR of SC	r_{cs}	5mohm
Voltage of SC	v_c	6v

system is shown as follows. When the wave energy generator provides sufficient input power, the load is powered by renewable energy sources while the energy storage system operates in the charging mode. During the charging process, the energy storage system is charged at the maximum input voltage in order to quickly reach a fully charged state. When the energy storage system is fully charged, it disconnects and waits to enter the discharging state. When the output power of the wave energy generator is not enough to supply the load, the energy storage system switches to the discharging mode. During the discharging process, the uiltimate goal is to ensure that the power from both SoC of each energy storage unit and the output power is balanced.

Case1: Since the wave energy power systems is reauired to supply energy to the load, the power generated should be more than the power consumed by the load. At this time, the energy storage unit is charging

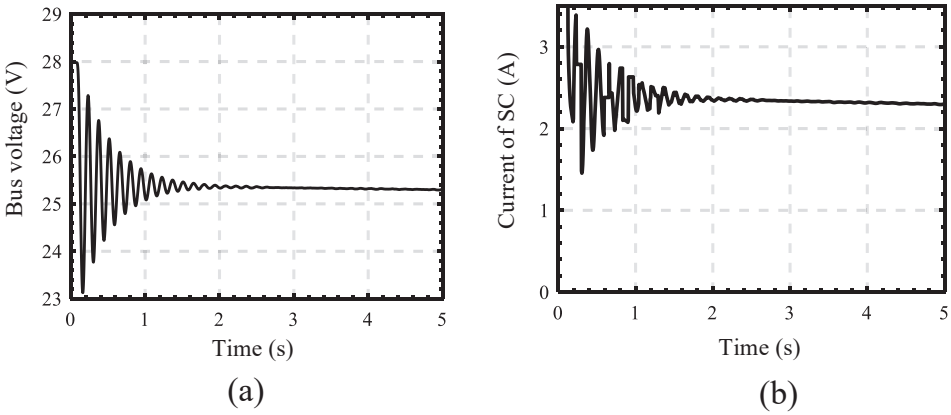

Fig. 19. (a) Bus voltage; (b) Current of SC under the conventional droop control.

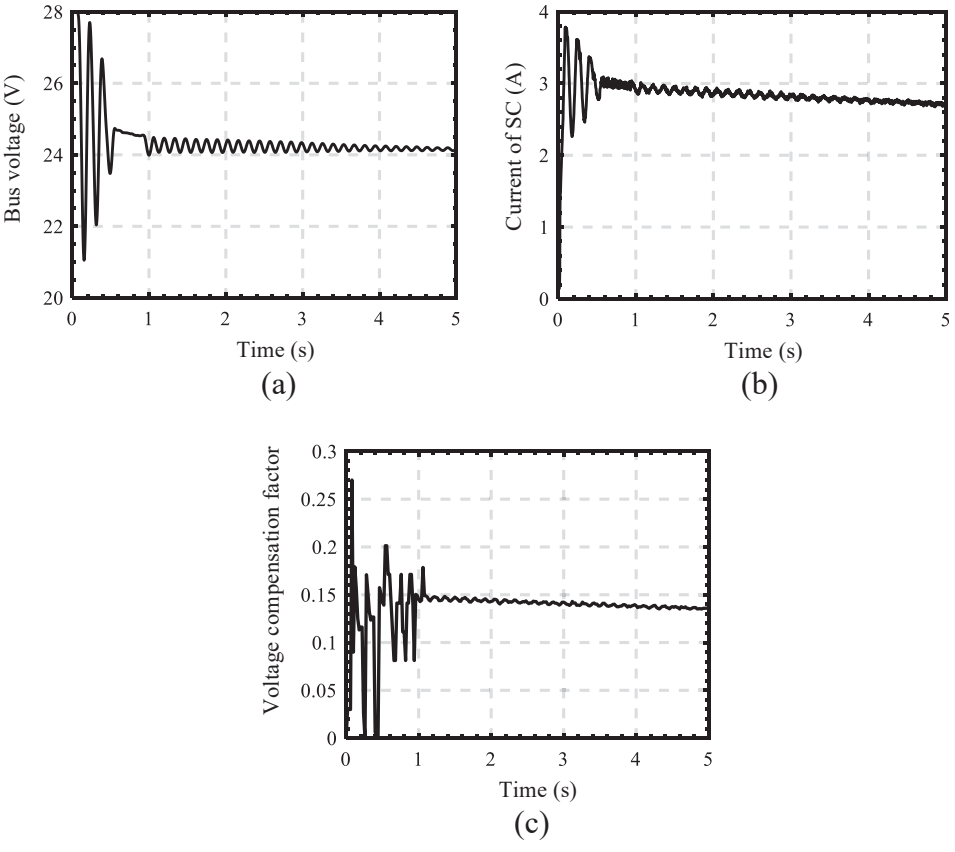

Fig. 20. (a) Bus voltage; (b) Current of SC; (c) Voltage compensation factor under the proposed droop control.

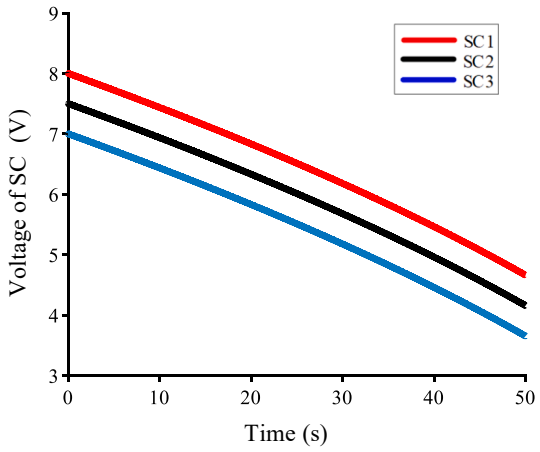

Fig. 21. SC voltage for conventional droop control.

and the output voltage of the wave energy generator is greater than 24 V. One of the more severe operating conditions is the charging of the energy storage unit under no load when the wave energy generation system starts to work. Because there is no load to consume the power at this time, and the initial voltage of the energy storage unit is 0 V, the charging current is high and the stability of the system is poor. In this paper, the output voltage of the wave energy generator is set to 28 V, and the experimental platform is configured to a single energy storage unit.

As shown in Fig. 19, under the conventional droop control, the bus voltage is greater than 25 V at th current of 2 A to 3 A. During the initial power-up, the bus voltage and the charging current of the energy storage unit fluctuated sharply, and the bus voltage stabilized at 1.52 s. At this time, the bus voltage fluctuation of the system decreases, and the charging current of the system gradually decreases as the SoC of the SC increases, therefore the voltage deviation due to the droop factor gradually decreases. The bus voltage converges to the reference value.

As shown in Fig. 20, the droop control strategy with the adaptive voltage compensation adjusts the voltage compensation coefficients through the primary and secondary differential information of the bus voltage. At 0.68 s, the fluctuation value of bus voltage is less than 5% and the system tends to reach a steady state. Since the voltage feedback factor changes with the fluctuation of the bus voltage, the bus voltage will fluctuate around 24 V after 0.68 s, and the adjustment time is reduced by 55.26%. When the voltage feedback factor stabilizes, the bus voltage and the charging current of the energy storage unit also approach to a steady state. At this time, the bus voltage fluctuation value of the system is less than 2%, which can provide a stable operating voltage for the load. Compared with the conventional droop control, the steady-state accuracy and regulation time of the system are substantially improved.

Case2: The LSRGs based wave energy generation system can improve the capacity of the energy storage system if more energy storage units are connected. However, the SoC of each energy storage unit is different, which will cause the overall energy storage system to work less efficiently, so energy equalization is required for each of the storage unit. In this paper, three energy storage units are designed to supply power to 30 W load under different initial voltage values. The capacity of three SC is 18F, the rated voltage is 10 V, and the initial voltages are 8, 7.5 and 7 V respectively.

As shown in Fig. 21, the energy from the storage units cannot be balanced under the conventional droop control. This is because the droop factor acts as a virtual resistance, which eliminates the influence of the line resistance, and thus the three SC will be powered with the same current. In contrast, the proposed adaptive voltage compensation controller introduces the terminal voltage of the SC, so that the SC with higher voltage generates more current. As shown in Fig. 22, the SC with the initial voltage of 8 V has the highest output current and the SC with voltage of 7 V has the lowest output current. The voltage of the SC gradually decreases and the output current gradually increases. At 40 s, the terminal voltage difference of three SCs is less than 0.1 V, which can be regarded as the energy storage unit to achieve energy balance.

5. Conclusion and discussion

The control chanlleges in the wave power generation and storage system of LSRG can be summarized as: (1) the large voltage drop due to low voltage and high current, and (2) the difficulty to achieve the power balance in the storage units. This paper proposes a novel droop control strategy with the adaptive voltage compensation. The proposed adapted control method can achieve power distribution according to the capacity of energy storage units with fast system response. In addition, increasing the bus voltage can decrease deviation and improve the self-recovery ability of the system when any interference is encountered, thus enhancing power supply quality. The algorithm proposed in this paper can improve the steady-state accuracy and regulation response time compared with the conventional droop control, under the low voltage and high current environment. The steady-state accuracy of the bus voltage based on the proposed adaptive voltage compensation control

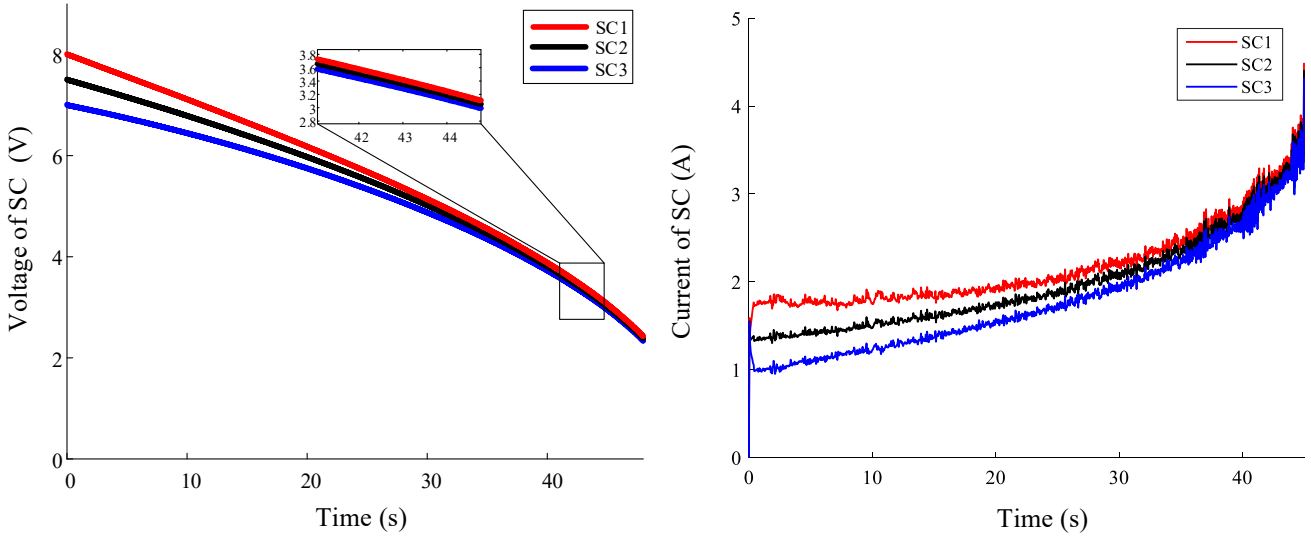

Fig. 22. SC voltage of adaptive voltage compensation droop control strategy.

strategy is improved and the adjustment time is reduced simultaneously. The SoC of the energy storage units can reach the balance state when the SoCs of the three energy storage units differ by 5%. The effectiveness and superiority of the proposed control method are verified experimentally.

Declaration of Competing Interest

The authors declare that they have no known competing financial interests or personal relationships that could have appeared to influence the work reported in this paper.

Acknowledgement

This work was supported in part by the National Science Foundation of China under Grant U1913214 and in part by the International Cooperation Program of Shenzhen Government GJHZ20200731095801004.

References

[1] Pan JF, Zou Y, Cheung N, Cao G. The direct-drive sensorless generation system for wave energy utilization. Int J Electr Power Energy Syst 2014;62:29–37. https://doi.org/10.1016/j.ijepes.2014.04.017.
[2] Huang L, Chen M, Wang L, Yue F, Guo R, Fu X. Analysis of a hybrid field-modulated linear generator for wave energy conversion. IEEE T Appl Supercon 2018;28(3):1–5. https://doi.org/10.1109/TASC.2018.2796549.
[3] Hong Y, Temiz I, Pan J, Eriksson M, Boström C. Damping studies on PMLG-based wave energy converter under oceanic wave climates. Energies 2021;14(4):920. https://doi.org/10.3390/en14040920.
[4] Yohanandhan RV, Elavarasan RM, Pugazhendhi R, Premkumar M, Mihet-Popa L, Zhao J, et al. A specialized review on outlook of future cyber-physical power system (CPPS) testbeds for securing electric power grid. Int J Electr Power Energy Syst 2022;136. https://doi.org/10.1016/j.ijepes.2021.107720.
[5] Pan JF, Li Q, Wu X, Cheung N, Qiu L. Complementary power generation of double linear switched reluctance generators for wave power exploitation. Int J Electr Power Energy Syst 2019;106:33–44. https://doi.org/10.1016/j.ijepes.2018.09.023.
[6] Wang H, Blaabjerg F. Reliability of capacitors for DC-link applications in power electronic converters—an overview. IEEE Trans on Ind Applicat 2014;50(5):3569–78.
[7] Oh YJ, Park JS, Hyon BJ, Lee J. Novel control strategy of wave energy converter using linear permanent magnet synchronous generator. IEEE T Appl Supercon 2018;28(3):1–5. https://doi.org/10.1109/TASC.2018.2799943.
[8] Huang L, Hu B, Hu M, Liu C, Zhu H. Research on primary excitation fully superconducting linear generators for wave energy conversion. IEEE T Appl Supercon 2019;29(5):1–5. https://doi.org/10.1109/TASC.2019.2903573.
[9] Xia T, Yu H, Guo R, Liu X. Research on the field-modulated tubular linear generator with quasi-halbach magnetization for ocean wave energy conversion. IEEE T Appl Supercon 2018;28(3):1–5. https://doi.org/10.1109/TASC.2018.2797959.
[10] Choi D-W, Byun S-I, Cho Y-H. A study on the maximum power control method of switched reluctance generator for wind turbine. IEEE T Magn 2014;50(1):1–4.
[11] Wang D, Shao C, Wang X, Zhang C. Performance characteristics and preliminary analysis of low cost tubular linear switch reluctance generator for direct drive WEC. IEEE T Appl Supercon 2016;26(7):1–5. https://doi.org/10.1109/TASC.2016.2599920.
[12] Lee G, Ko B, Cho J, Kim R. A distributed control method based on a voltage sensitivity matrix in DC microgrids with low-speed communication. IEEE T Smart Grid 2019;10(4):3809–17. https://doi.org/10.1109/TSG.2018.2835811.
[13] Bin Shaheed MN, Sozer Y, Chowdhury S, De Abreu-Garcia JA. A Novel decentralized adaptive droop control technique for DC microgrids based on integrated load condition processing. IEEE 2020:2095–100.
[14] Huang P, Liu P, Xiao W, El Moursi MS. A novel droop-based average voltage sharing control strategy for DC microgrids. IEEE T Smart Grid 2015;6(3):1096–106. https://doi.org/10.1109/TSG.2014.2357179.
[15] Sun F, Yang P, Zhu J, Zhao H, Yu M, Wei W. A two-stage improved droop control method for economic operation of islanded DC microgrids. IEEE 2019:3116–21.
[16] Augustine S, Mishra MK, Lakshminarasamma N. A unified control scheme for a standalone solar-PV low voltage dc microgrid system with HESS. IEEE J. Emerg. Select. Top. Power Electron. 2020;8(2):1351–60.
[17] Liu C, Zhao J, Wang S, Lu W, Qu K. Active identification method for line resistance in DC microgrid based on single pulse injection. IEEE T Power Electr 2018;33(7):5561–4. https://doi.org/10.1109/TPEL.2017.2784565.
[18] Shivam, Dahiya R. Intelligent distributed control techniques for effective current sharing and voltage regulation in DC distributed systems. Arab J Sci Eng 2017;42(12):5071–81.
[19] Davari M, Mohamed YAI. Robust droop and DC-bus voltage control for effective stabilization and power sharing in VSC multiterminal DC grids. IEEE T Power Electr 2018;33(5):4373–95. https://doi.org/10.1109/TPEL.2017.2715039.
[20] Mokhtar M, Marei MI, El-Sattar AA. An adaptive droop control scheme for DC microgrids integrating sliding mode voltage and current controlled boost converters. IEEE T Smart Grid 2019;10(2):1685–93.
[21] Sun C, Joos G, Bouffard F. Adaptive coordination for power and SoC limiting control of energy storage in an islanded AC microgrid with impact load. IEEE T Power Deliver 2020;35(2):580–91.
[22] Li D, Wu Z, Zhao B, Zhang L. An improved droop control for balancing state of charge of battery energy storage systems in AC microgrid. IEEE Access 2020;8:71917–29. https://doi.org/10.1109/ACCESS.2020.2987098.
[23] Guo F, Wen C, Mao J, Song Y. Distributed secondary voltage and frequency restoration control of droop-controlled inverter-based microgrids. IEEE T Ind Electron 2015;62(7):4355–64. https://doi.org/10.1109/TIE.2014.2379211.
[24] Che L, Shahidehpour M. DC microgrids: economic operation and enhancement of resilience by hierarchical control. IEEE T Smart Grid 2014;5(5):2517–26. https://doi.org/10.1109/TSG.2014.2344024.
[25] Shafiee Q, Dragicevic T, Vasquez JC, Guerrero JM. Hierarchical control for multiple DC-microgrids clusters. IEEE T Energy Conver 2014;29(4):922–33. https://doi.org/10.1109/TEC.2014.2362191.
[26] Jin C, Wang P, Xiao J, Tang Y, Choo FH. Implementation of hierarchical control in DC microgrids. IEEE T Ind Electron 2014;61(8):4032–42. https://doi.org/10.1109/TIE.2013.2286563.
[27] Guo F, Xu Q, Wen C, Wang L, Wang P. Distributed secondary control for power allocation and voltage restoration in islanded DC microgrids. IEEE T Sustain Energ 2018;9(4):1857–69. https://doi.org/10.1109/TSTE.2018.2816944.
[28] Sadabadi MS. Line-independent plug-and-play voltage stabilization and L_2 gain performance of DC microgrids. IEEE Control Syst. Lett. 2021;5(5):1609–14. https://doi.org/10.1109/LCSYS.2020.3041335.
[29] Tah A, Das D. An enhanced droop control method for accurate load sharing and voltage improvement of isolated and interconnected DC microgrids. IEEE T Sustain Energ 2016;7(3):1194–204. https://doi.org/10.1109/TSTE.2016.2535264.
[30] Liu G, Mattavelli P, Saggini S. Resistive–capacitive output impedance shaping for droop-controlled converters in DC microgrids with reduced output capacitance. IEEE T Power Electr 2020;35(6):6501–11.
[31] Pradhan S, Singh B, Panigrahi BK, Murshid S. A composite sliding mode controller for wind power extraction in remotely located solar PV–wind hybrid system. IEEE T Ind Electron 2019;66(7):5321–31. https://doi.org/10.1109/TIE.2018.2868009.
[32] Zhang Z, Guan C, Liu Z. Real-time optimization energy management strategy for fuel cell hybrid ships considering power sources degradation. IEEE Access 2020;8:87046–59.